Supramolecular Nanostructures

DOI: 10.1002/anie.200603629

Formation of Vesicular Structures through the Self-Assembly of a Flexible Bis-Zwitterion in Dimethyl Sulfoxide**

Carsten Schmuck, Thomas Rehm, Katja Klein, and Franziska Gröhn*

Dedicated to Professor Manfred Christl on the occasion of his 65th birthday

The controlled self-assembly of flexible molecules can give rise to large aggregates with new and interesting properties that the underlying monomers do not have. Nature uses this principle widely; the self-assembled protein core of the tobacco mosaic virus and the formation of a bilayer from the self-assembly of an amphiphilic phospholipids are prominent examples.[1] In the last few years, a variety of artificial systems have been designed that also form large aggregates through the noncovalent self-assembly of small monomers. For example, the four H-bonded supramolecular helical polymer rods described by Meijer and co-workers attracted much attention in this context.[2] The hydrophobic collapse of peptide amphiphiles as introduced by Stupp and co-workers leads to large cylindrical nanostructures that can be used as templates for organic–inorganic hybrid materials.[3] Also, the formation of preorganized antiparallel β sheets can lead to highly ordered aggregates as Matsuura et al. recently showed through the introduction of an artificial peptide nanosphere.[4a]

Of self-assembled supramolecular structures, vesicles are of particular interest owing to their potential application as carrier systems. Several vesicle-forming systems beyond simple lipids have been investigated based on building blocks ranging from polymers to polypeptides and more-complex structures.[4a] For example, Meijer and co-workers used a cyano derivative for their oligo(*p*-phenylene vinylene) building block to form well-defined vesicular structures.[5] Rotello and co-workers used a DNA-binding motif to cause statistical copolymers to form vesicular structures,[5b] whereas Schlaad and co-workers used polyelectrolyte complex formation of hydrophilic copolymers to form vesicles.[5c] A recent overview on vesicle formation and applications is given by Antonietti and Förster.[5d] They emphasize that in addition to the building-block geometry (surface-to-volume ratio), secondary forces such as hydrogen bonding between building blocks can enforce the formation of vesicles.

One of the advantages of polymeric vesicles as opposed to classical surfactant or lipid vesicles is the broader range of solvents and temperature that is accessible. Furthermore, small-lipid vesicles often represent kinetically controlled structures because the lipid building block is not molecularly soluble in the solvent. In this respect, the investigation of vesicle formation of small building blocks other than classical lipids is of high interest as they may have the above-mentioned advantages over simple lipid vesicles. However, most of the vesicle-forming systems reported so far that function in polar solvents rely on weak aromatic stacking, extensive hydrophobic contacts, or the much stronger metal–ligand interactions as the main driving force for self-assembly.[6] We are currently exploring how charge interactions can be used in this context for the formation of large aggregates through the self-assembly of zwitterionic monomers in polar solvents.[7] We have recently shown that a self-complementary bis-zwitterion with a hydrophilic flexible triethylene glycol linker between the two zwitterions forms cyclic nanometer-sized dimers even in aqueous dimethyl sulfoxide (DMSO).[8] We now report herein that bis-zwitterion **1** with a lipophilic alkyl linker in between the two charged binding sites forms large vesicular structures.

The synthesis of bis-zwitterion **1** is shown in Scheme 1. 6-Aminocaproic acid methyl ester **3** was attached to the pyrrole benzyl ester **2** through activation of the guanidino group by triflic anhydride. After hydrolysis of the methyl ester group in **4**, the resulting free acid **5** was reacted with 0.5 equivalents of 1,2-diaminoethane **6**. Deprotection of **7** first with H_2/Pd and then with trifluoroacetic acid (TFA) provided, after pH adjustment, the flexible bis-zwitterion **1** in 99% yield.

Upon dissolution in DMSO, zwitterion **1** forms a colloidal solution at higher concentrations and shows an extensive Tyndall effect at room temperature. However, these concentrated solutions were only stable for some hours. Upon prolonged standing, **1** started to precipitate as a white fluffy deposit. Quantitative NMR dilution spectroscopic studies showed that in the concentration range from 0.5 to 50 mM two different signal sets can be observed (Figure 1). The relative intensity of these two signals is concentration-dependent, indicating a dynamic equilibrium in solution. To obtain

[*] Prof. Dr. C. Schmuck, Dipl.-Chem. T. Rehm
Institut für Organische Chemie
Universität Würzburg
Am Hubland, 97074 Würzburg (Germany)
Fax: (+49) 931-888-4625
E-mail: schmuck@chemie.uni-wuerzburg.de
K. Klein, Dr. F. Gröhn
Max-Planck-Institut für Polymerforschung
Ackermannweg 10, 55128 Mainz (Germany)

[**] We thank Prof. Dr. Frank Würthner and Dr. Marina Lysetska (Universität Würzburg, Institut für Organische Chemie) for the AFM measurements and helpful discussions. Ongoing financial support of our work by the Deutschen Forschungsgemeinschaft (DFG) and the Fonds der Chemischen Industrie is gratefully acknowledged. We thank Dr. Peter Lindner and Dr. Ralf Schweins for help with the SANS measurements at ILL, Grenoble, and the ILL for financial support.

Supporting information for this article is available on the WWW under http://www.angewandte.org or from the author.

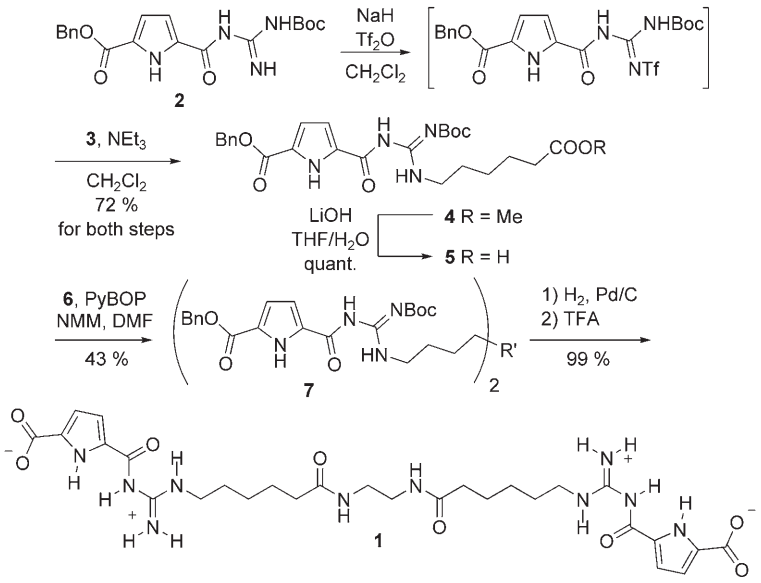

Scheme 1. Synthesis of the amphiphilic zwitterion **1**. Boc = *tert*-butyloxycarbonyl, PyBOP = benzotriazol-1-yloxytripyrrolidinophosphonium hexafluorophosphate, DMF = *N*,*N*-dimethylformamide, NMM = *N*-methylmorpholine, Tf = trifluoromethanesulfonyl.

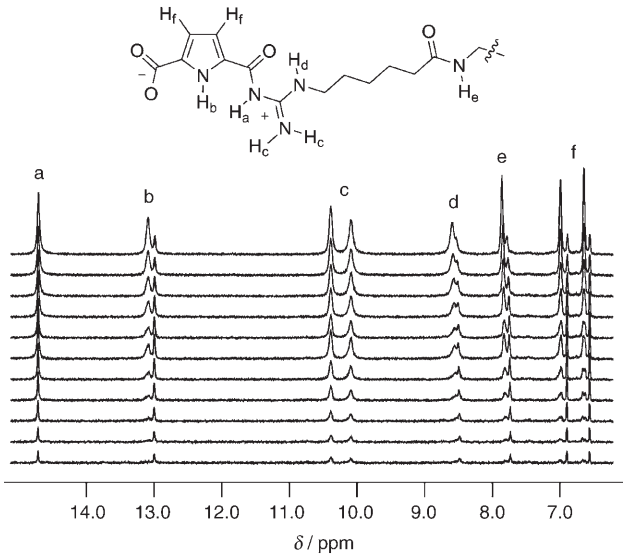

Figure 1. NMR dilution spectroscopic study in DMSO in the concentration range from 50 mM (top) to 0.5 mM (bottom).

information on the size of these two particles, DOSY NMR spectroscopic experiments were performed, which confirmed the coexistence of the monomer and a dimer of **1** in solution. Both a concentrated (30 mM) and a diluted (1 mM) sample of **1** as well as the protected monomer **7** (1 mM) were examined. The data show that both the zwitterionic species **1** present at low concentrations and the protected monomer **7**, which cannot self-assemble under these conditions owing to the lack of charges, have similar diffusion coefficients $D(\mathbf{7}) = 1.4 \times 10^{-10}\ m^2 s^{-1}$ and $D(\mathbf{1}) = 1.1 \times 10^{-10}\ m^2 s^{-1}$. The corresponding hydrodynamic radii calculated by using the Stokes equation are 0.78 nm for **7** and 0.98 nm for **1**.[9] For the species present at larger concentrations of zwitterion **1**, the diffusion coefficient decreased to a value of $D(\mathbf{1}) = 0.8 \times 10^{-10}\ m^2 s^{-1}$, the corresponding hydrodynamic radius ($r_H = 1.42$ nm) being significantly larger. This clearly shows that **1** exists in a concentration-dependent dynamic monomer–dimer equilibrium in solution as shown schematically in Figure 2.

However, the strong Tyndall effect indicates that even larger aggregates than cyclic dimers must be present in concentrated solutions. Indeed, dynamic light scattering (DLS) experiments confirmed the presence of distinct large aggregates of approximately 150 nm in size in addition to small amounts of much larger structures at a size of around 5 μm. The larger aggregates seem to form from the 150 nm sized particles in a dynamic equilibrium. Even if these large aggregates are removed from the solution by filtration or centrifugation, they reform upon standing. The intensity-weighted distribution of hydrodynamic radii is shown in Figure 3. In light scattering, even a few larger particles contribute strongly to the scattering intensity and thus the distribution. Assuming both species consist of the same material and are homogeneous,[10] the intensity-weighted distribution can be transformed into a number distribution: In solution, only a very small fraction (ca. 10^{-8}) of particles are of the 5-μm size and hence the majority of particles are of the 150-nm size. However, regarding the number of zwitterionic

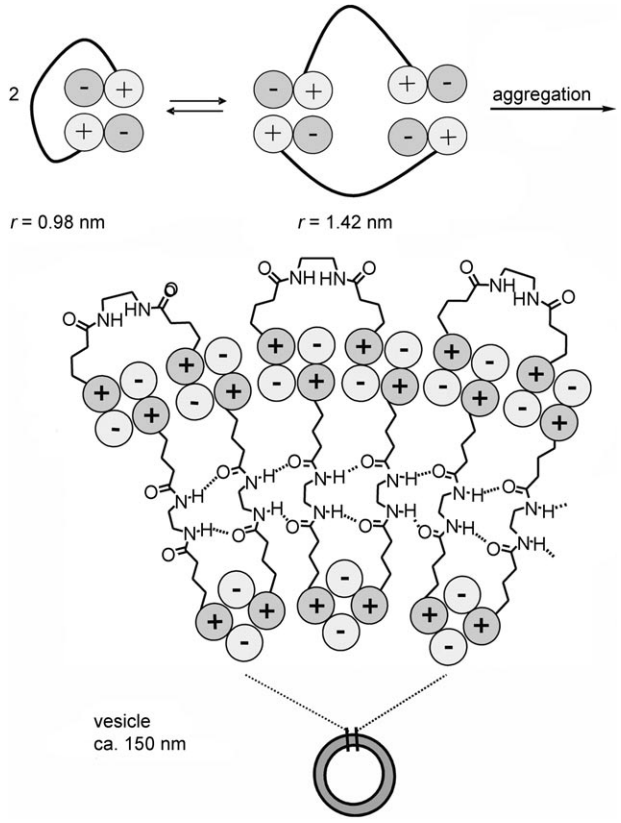

Figure 2. Bis-zwitterion **1** in solution forms cyclic dimers, which then self-assemble into large vesicles.

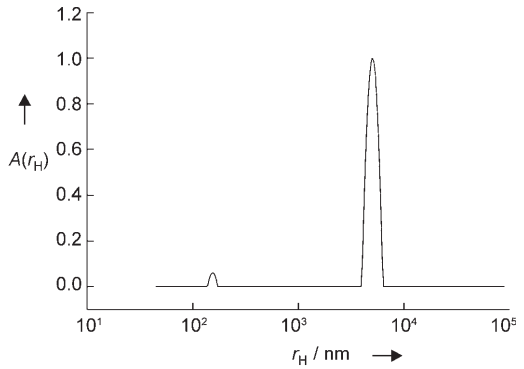

Figure 3. Intensity-weighted distribution of hydrodynamic radii as determined by dynamic light scattering in DMSO; [**1**] = 2 mM. r_H = hydrodynamic radius.

monomers forming these species, of course the larger amount is found inside the large particles (about 85% if they were homogeneous).

The nature of these aggregates was then further investigated by atomic force microscopy (AFM). The AFM image in Figure 4A shows individual spherical particles of approximately 140 nm in diameter and about 6–7 nm in height, which then further self-assemble into much larger aggregates with a size greater than 1 μm. This is in good agreement with the light-scattering data in solution. Owing to the loss of solvent particles, images by AFM show, in general, slightly smaller diameters than DLS.[11] The contour plot of the 140 nm sized spherical particles (Figure 4B) is consistent with a vesicular structure. In solution, a vesicle forms a hollow sphere, which in the AFM experiment is distorted by the interaction with the surface. This flattening process of the vesicle membrane leads to the formation of shoulders as seen in the contour plot, whereas the inner part of the vesicle, filled with solvent, is altered to an ellipsoid (schematically shown in Figure 4B).

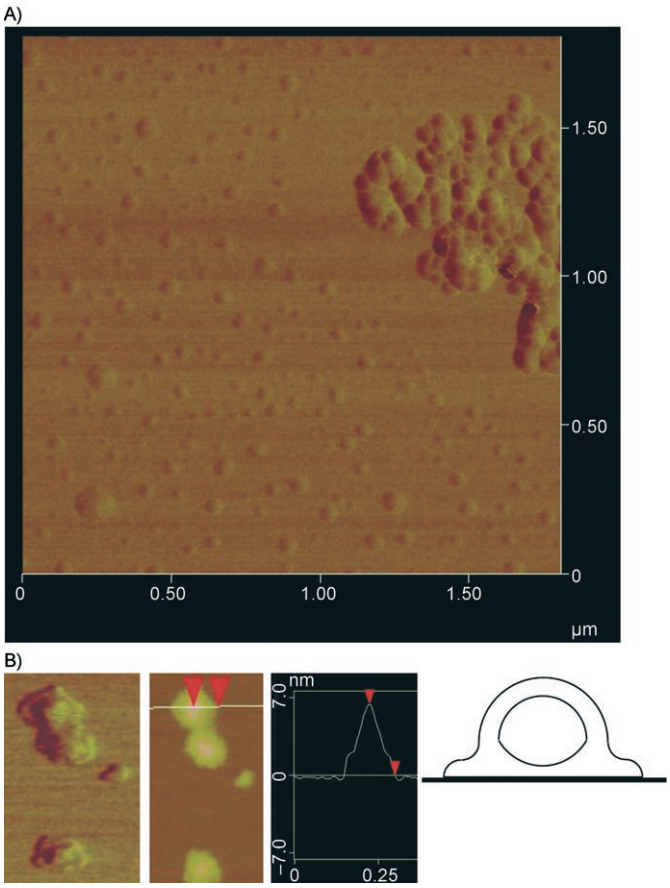

Figure 4. A) AFM image of **1** on mica showing approximately 150 nm sized vesicles and their aggregation into even larger aggregates. B) Phase and height image of a typical vesicle and its schematic illustration based on the section plot (horizontal scale in μm, vertical scale in nm). The red markers indicate corresponding areas in the plots.

To further confirm that indeed vesicular aggregates are present in solution, we also performed small-angle neutron scattering (SANS) experiments. Scattering experiments were performed in a concentration range of **1** from 2–15 mM in [D_6]DMSO with a wavelength of 6 Å and a wavelength spread of 11%. Within this concentration range, in all cases, aggregates are present that are too large as to be completely analyzed by small-angle scattering, that is, no Guinier regime can be reached. This is expected from the above-mentioned DLS and AFM results. However, the neutron-scattering data provide valuable information about the internal structure of the aggregates observed both in solution (DLS) as well as in the AFM imaging. A Thickness–Guinier plot (Figure 5) of

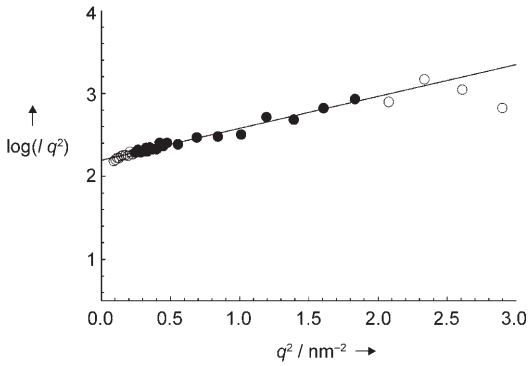

Figure 5. Thickness–Guinier plot from data of a 4 mM solution of **1** in [D_6]DMSO as obtained from SANS measurements. Data points of the linear regime used for the Guinier fit are plotted as filled symbols.

$I(q)q^2$ versus q^2 (I = scattering curve, q = scattering wave vector magnitude) shows a linear behavior in the appropriate q range confirming the presence of vesicle walls with a thickness radius of gyration of $r_{G,t} = 0.9$ nm.[12] Assuming that the lamellae has a homogeneous scattering contrast in SANS, which is reasonable due to the chemical structure of the zwitterion, the $r_{G,t}$ translates into an average lamellae thickness of $d = 3.1$ nm.

Further details about the nature of the vesicle wall can be obtained by calculating the thickness density profile $\rho(x)$ of the lamellae through the thickness pair distance distribution function $P_t(r)$, which basically represents a distance histogram in real space.[13] This analysis confirms the average thickness of the lamellae of about 3.4 nm (Figure 6 A). The $P_t(r)$ shown

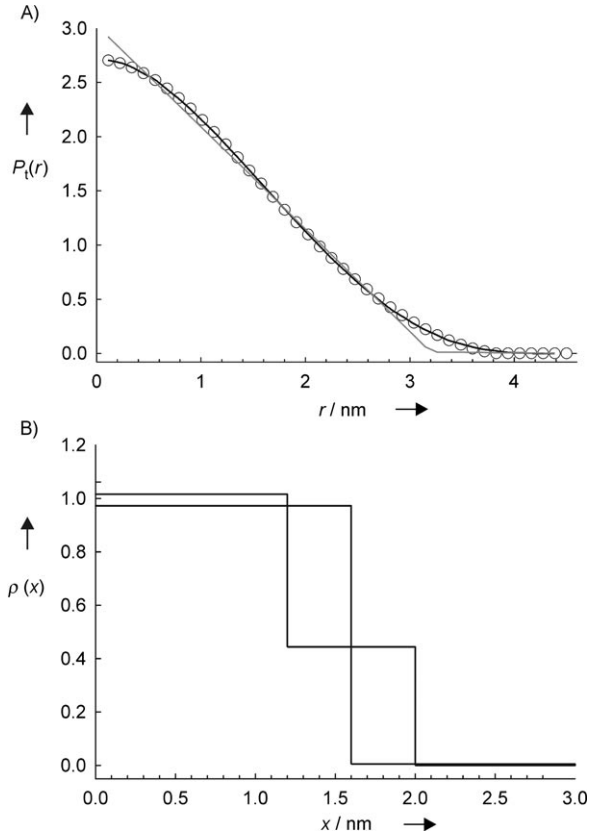

Figure 6. A) Transversal pair distance distribution function resulting from the Fourier transformation of the experimental SANS data (circles). The gray line represents the fit of the data corresponding to a one-step transversal density profile, whereas the black line corresponds to a two-step transversal density profile. B) Transversal density profile corresponding to the gray and the black curve in the top plot. $P_t(r)$ = thickness pair distance distribution function, $\rho(x)$ = transversal difference scattering length density profile, x = vesicle-wall thickness.

has a $r_{G,t}$ of 0.9 nm, which is in very good agreement with the Thickness–Guinier plot. We find that the experimental data (Figure 6A) can be very well described by a two-step density profile for the lamellae as is shown by the black curve, whereas a simple one-step profile fails to reproduce the $P_t(r)$ data points accurately (gray line).[13] Hence, the wall of the vesicles is not completely homogeneous but is built up from two different parts with two different thicknesses.[14] The thinner part has a thickness of $d = 2.4$ nm and the thicker part has $d = 4$ nm (Figure 6B: transversal radius of gyration $r_{G,t} =$ 1.2 and 2 nm for the thin and thick portion of the vesicle walls, respectively). However, no larger wall thickness is detected. Hence, the scattering results clearly prove the existence of hollow vesicles as opposed to multilameller onionlike structures, again in agreement with the AFM results.

The two-step profile as extracted from the SANS data might be explained by a main vesicle wall with a thickness of 2.4 nm built by a monolayer of self-assembled zwitterions **1**. At some areas, the lamellae is thicker owing to stacking of a second layer of zwitterions, either as another double wall, or more likely as single monomers forming loops on the surface as depicted in Figure 2. According to simple force-field calculations, such an arrangement would have exactly the molecular dimensions as experimentally determined from the SANS measurements. Within the monolayer of the vesicle wall, the zwitterions **1** have a calculated length of approximately 2.5 nm, whereas the additional loop extends the thickness of the wall to about 3.9 nm according to the calculations.[15]

Hence, all the experimental data clearly prove the formation of large vesicles through the hierachical self-assembly of zwitterion **1** as depicted in Figure 2. First, at lower concentrations two monomers interact to form cyclic dimers as indicated by the NMR dilution and DOSY NMR spectroscopic studies. Owing to the nonpolar nature of the linker, these dimers then start to self-assemble. The major driving force for the formation of self-assembled monolayers is most likely H-bonds between the amide groups in the middle of the alkyl chains together with van der Waals interactions between neighboring chains. Additional monomers then interact with the zwitterionic binding sites on the outer side of these monolayers, inducing a curvature and hence the formation of spherical vesicles. These vesicles can then further aggregate (perhaps through the alkyl loops on their surface) to form even larger structures as seen in the AFM image and the DLS experiments. Eventually, these larger aggregates precipitate from solution.

In conclusion, we have shown herein that the flexible bis-zwitterion **1** can self-assemble even in polar solution to form large vesicular structures. Vesicle formation is driven by the amphiphilic nature of zwitterion **1**: The zwitterionic binding sites provide the main binding energy to allow self-assembly even in DMSO, and the nonpolar alkyl linker determines the specific mode of aggregation. This also explains the different self-assembly behavior of **1** compared with the previously reported zwitterion with a hydrophilic spacer that does not form vesicles but just cyclic dimers.[8] Hence, a further variation of the linker in between the two zwitterionic binding motifs will most likely again lead to different aggregation modes that eventually allow the controlled formation of specific nanostructures in polar solution.

Received: September 5, 2006
Revised: November 14, 2006
Published online: January 17, 2007

Keywords: ion-pair formation · self-assembly · supramolecular chemistry · vesicles · zwitterions

[1] a) A. Klug, *Philos. Trans. R. Soc. London Ser. B* **1999**, *354*, 531–535; b) T. L. Schlick, Z. Ding, E. W. Kovacs, M. B. Francis, *J. Am. Chem. Soc.* **2005**, *127*, 3718–3723.
[2] F. J. M. Hoeben, P. Jonkheijm, E. W. Meijer, A. H. P. J. Schenning, *Chem. Rev.* **2005**, *105*, 1491–1546.
[3] J. Hartgerink, E. Beniash, S. Stupp, *Science* **2001**, *294*, 1684–1688.
[4] a) K. Matsuura, K. Murasato, N. Kimizuka, *J. Am. Chem. Soc.* **2005**, *127*, 10148–10149; b) L. F. Zhang, A. Eisenberg, *Science* **1995**, *268*, 1728–1731; c) D. E. Discher, A. Eisenberg, *Science* **2002**, *297*, 967–973; d) B. M. Discher, Y. Y. Won, D. S. Ege, J. C. M. Lee, F. S. Bates, D. E. Discher, D. A. Hammer, *Science* **1999**, *284*, 1143–1146; e) H. Kukula, H. Schlaad, M. Antonietti, S. Förster, *J. Am. Chem. Soc.* **2002**, *124*, 1658–1663; f) U.

Borchert, U. Lipprandt, M. Bilang, A. Kimpfler, A. Rank, R. Peschka-Suss, R. Schubert, P. Lindner, S. Förster, *Langmuir* **2006**, *22*, 5843 – 5847; g) J. Bang, S. M. Jain, Z. B. Li, T. P. Lodge, J. S. Pedersen, E. Kesselman, Y. Talmon, *Macromolecules* **2006**, *39*, 1199 – 1208.

[5] a) F. J. M. Hoeben, I. O. Shklyarevski, M. J. Pouderoijen, H. Engelkamp, A. H. P. J. Schenning, P. C. M. Christianen, J. C. Maan, E. W. Meijer, *Angew. Chem.* **2006**, *118*, 1254 – 1258; *Angew. Chem. Int. Ed.* **2006**, *45*, 1232 – 1236; b) F. Ilhan, T. H. Galow, M. Gray, G. Clavier, V. M. Rotello, *J. Am. Chem. Soc.* **2000**, *122*, 5895 – 5896; c) S. Schrage, R. Sigel, H. Schlaad, *Macromolecules* **2003**, *36*, 1417 – 1420; d) M. Antonietti, S. Förster, *Adv. Mater.* **2003**, *15*, 1323 – 1333.

[6] a) J.-M. Lehn, *Supramolecular Chemistry. Concepts and Perspectives*, Wiley-VCH, Weinheim, **1995**; b) H.-J. Schneider, *Principles and Methods in Supramolecular Chemistry*, Wiley-VCH, Weinheim, **2000**.

[7] a) C. Schmuck, W. Wienand, *J. Am. Chem. Soc.* **2003**, *125*, 452 – 459; b) S. Schlund, C. Schmuck, B. Engels, *J. Am. Chem. Soc.* **2005**, *127*, 11115 – 11124.

[8] C. Schmuck, T. Rehm, K. Gröhn, K. Klein, F. Reinhold, *J. Am. Chem. Soc.* **2006**, *128*, 1430 – 1431.

[9] Y. Cohen, L. Avram, L. Frish, *Angew. Chem.* **2005**, *117*, 524 – 560; *Angew. Chem. Int. Ed.* **2005**, *44*, 520 – 544.

[10] As will be discussed below, the particles are not completely homogenous. But it seems useful to use this simplification as a first approximation to arrive at an estimate for particle distribution.

[11] a) E. Minatti, P. Viville, R. Borsali, M. Schappacher, A. Deffieux, R. Lazzaroni, *Macromolecules* **2003**, *36*, 4125 – 4133; b) N. Ouarti, P. Viville, R. Lazzaroni, E. Minatti, M. Schappacher, A. Deffieux, R. Borsali, *Langmuir* **2005**, *21*, 1180 – 1186.

[12] *Neutron, X-rays and Light: Scattering Methods Applied to Soft Condensed Matter* (Eds.: P. Lindner, T. Zemb), Elsevier, Dordrecht, **2002**.

[13] a) O. Glatter, *Acta Phys. Austriaca* **1977**, *47*, 83 – 102; O. Glatter, *J. Appl. Crystallogr.* **1977**, *10*, 415 – 421; b) O. Glatter, *J. Appl. Crystallogr.* **1980**, *13*, 7 – 11; O. Glatter, *J. Appl. Crystallogr.* **1980**, *13*, 577 – 584; c) O. Glatter, *J. Appl. Crystallogr.* **1981**, *14*, 101 – 108; d) O. Glatter, B. Hainisch, *J. Appl. Crystallogr.* **1984**, *17*, 435 – 441; e) O. Glatter, *J. Appl. Crystallogr.* **1988**, *21*, 886 – 890; f) D. J. Iampietro, L. L. Brasher, E. W. Kaler, A. Stradner, O. Glatter, *J. Phys. Chem. B* **1998**, *102*, 3205 – 3213; g) F. Gröhn, B. J. Bauer, E. J. Amis, *Macromolecules* **2001**, *34*, 6701 – 6707.

[14] As the scattering contrast of the different molecule parts is very similar, this is not sufficient to account for a step in the density profile and the profile has to be caused by parts of different thickness.

[15] For details of the calculations and graphical representations of the energy-minimized structures of the cyclic monomer and dimer of **1** as well as a nonamer as a model for the vesicle wall, see the Supporting Information.

